# On-axis and far-field sound radiation from resilient flat and dome-shaped radiators

Ronald M. Aarts[a] and Augustus J. E. M. Janssen[b]
*Philips Research Europe, HTC 36 (WO-02), NL-5656AE Eindhoven, The Netherlands*

(Received 25 July 2008; revised 23 December 2008; accepted 24 December 2008)

On-axis and far-field series expansions are developed for the sound pressure due to an arbitrary, circular symmetric velocity distribution on a flat radiator in an infinite baffle. These expansions are obtained by expanding the velocity distributions in terms of orthogonal polynomials $R_{2n}^0(\sigma/a) = P_n(2(\sigma/a)^2-1)$ with $P_n$ the Legendre polynomials. The terms $R_{2n}^0$ give rise to a closed-form expression for the pressure on-axis as well as for the far-field pressure. Furthermore, for a large number of velocity profiles, including those associated with the rigid piston, the simply supported radiator, and the clamped radiators as well as Gaussian radiators, there are closed-form expressions for the required expansion coefficients. In particular, for the rigid, simply supported, and clamped radiators, this results in explicit finite-series expressions for both the on-axis and far-field pressures. In the reverse direction, a method of estimating velocity distributions from (measured) on-axis pressures by matching in terms of expansion coefficients is proposed. Together with the forward far-field computation scheme, this yields a method for far-field loudspeaker assessment from on-axis data (generalized Keele scheme). The forward computation scheme is extended to dome-shaped radiators with arbitrary velocity distributions. © *2009 Acoustical Society of America.*
[DOI: 10.1121/1.3075594]

PACS number(s): 43.38.Ar, 43.20.Bi, 43.40.At, 43.20.Px [AJZ] Pages: 1444–1455

## I. INTRODUCTION

In this paper a new analytic method for the calculation of on-axis and far-field sound pressures is presented. The theory of sound radiation from a flat or dome-shaped radiator in a rigid infinite baffle until 1980 is broadly reviewed by Harris[1] while a whole set of analytic results for the circular symmetric flat piston radiator has been given by Greenspan.[2] Recent analytical and/or numerical efforts have been undertaken by Mast and Yu,[3] Hansen,[4] Mellow,[5] and Kelly and McGough,[6] to name just a few. The point of view taken in the present paper, viz., the applications to sound radiation of the analytical results as developed in the diffraction theory of optical aberrations by Nijboer[7] and Zernike and Nijboer[8] (also see Refs. 9 and 10) is, however, apparently new. Using this new approach, many of the analytic results in Ref. 2, such as those on on-axis pressure and those on reaction on radiator and on radiated power, and the results in textbooks[11] on far-field expressions and directivity can be presented and extended in a systematic fashion. The aim of the present paper is to work out this approach for the results on on-axis pressure and far-field expressions for arbitrary velocity distributions on both flat piston radiators and dome-shaped radiators. The radiated pressure is given in integral form by the Rayleigh integral[11,12] as

$$p(\underline{r},t) = \frac{i\rho_0 ck}{2\pi} e^{i\omega t} \int_S v(\underline{r}_s) \frac{e^{-ikr'}}{r'} dS, \tag{1}$$

where $\rho_0$ is the density of the medium, $c$ is the speed of sound in the medium, $k=\omega/c$ is the wave number, and $\omega$ is the radian frequency of the vibrating surface $S$. Furthermore $t$ is time, $\underline{r}$ is a field point, $\underline{r}_s$ is a point on the surface $S$, $r' = |\underline{r}-\underline{r}_s|$ is the distance between $\underline{r}$ and $\underline{r}_s$, and $v(\underline{r}_s)$ is the normal component of a (not necessarily uniform) velocity profile on the surface $S$. The time variable $t$ in $p(\underline{r},t)$ and the harmonic factor $\exp(i\omega t)$ in front of the integral in Eq. (1) will be omitted in the sequel. For transparency of exposition, the surface $S$ is assumed initially to be a disk of radius $a$, $|\underline{r}_s| = r_s \leq a$, with average velocity $V_s$; later on, generalization to the case of dome-shaped radiator surfaces $S$ is done. See Fig. 1 for the geometry and notations used in the case of a flat piston. The volume velocity at the piston is

$$\int_S v(\underline{r}_s) dS = V_s \pi a^2. \tag{2}$$

Frankort[13] showed that loudspeaker cones mainly vibrate in a radially symmetric fashion. Therefore the attention in this paper is restricted to radially symmetric velocity distributions $v$, which are denoted as $v(\sigma)$, $0 \leq \sigma \leq a$. Under an integrability condition, viz., $\int_S |v(\underline{r}_s)|^2 dS < \infty$, these $v$'s admit a representation

$$v(\sigma) = V_s \sum_{n=0}^{\infty} u_n R_{2n}^0(\sigma/a), \quad 0 \leq \sigma \leq a, \tag{3}$$

in which

[a]Electronic mail: ronald.m.aarts@philips.com. Also at Technical University Eindhoven, Den Dolech 2, PT3.23, P.O Box 513, NL-5600 MB Eindhoven, The Netherlands.
[b]Electronic mail: a.j.e.m.janssen@philips.com

 0001-4966/2009/125(3)/1444/12/$25.00 

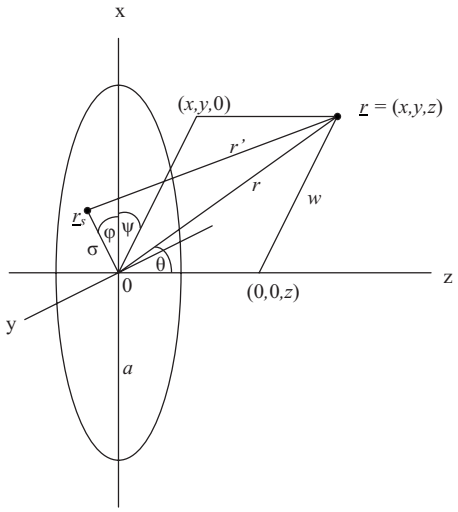


FIG. 1. Setup and notations.

$$\underline{r}_s = (x_s, y_s, 0) = (\sigma \cos\varphi, \sigma \sin\varphi, 0),$$

$$\underline{r} = (x, y, z) = (r \sin\theta \cos\psi, r \sin\theta \sin\psi, r \cos\theta),$$

$$w = r \sin\theta = (x^2 + y^2)^{1/2}, \quad z = r \cos\theta,$$

$$r = |\underline{r}| = (x^2 + y^2 + z^2)^{1/2} = (w^2 + z^2)^{1/2},$$

$$r' = |\underline{r} - \underline{r}_s| = (r^2 + \sigma^2 - 2\sigma w \cos(\psi - \varphi))^{1/2}$$

$$R_{2n}^0(\rho) = P_n(2\rho^2 - 1), \quad 0 \le \rho \le 1, \tag{4}$$

where $P_n$ are the Legendre polynomials.[14] [The notation $R_{2n}^0(\rho)$ stems from the analytical theory of optical aberrations.[7–9]] The main aim of the present paper is to establish analytical results for the on-axis and far-field pressures $p(\underline{x})$ in Eq. (1) related to the coefficients $u_n$ and polynomials $R_{2n}^0$ occurring in the expansion in Eq. (3).

By orthogonality of the terms $R_{2n}^0(\rho)$, the coefficients $u_n$ in Eq. (3) can be found in integral form as

$$u_n = \frac{2(2n+1)}{V_s} \int_0^1 R_{2n}^0(\rho) v(a\rho) \rho d\rho, \quad n = 0, 1, \ldots . \tag{5}$$

An expansion of the type as in Eq. (3) is usually referred to as a Zernike$^0$ expansion; in this paper only azimuthal order $m=0$ occurs, and so the superscript 0 is dropped. There is an impressive number of cases where one can explicitly find the $u_n$ in Eq. (5); some of these appear in the present paper and include the rigid, simply supported, and clamped radiators

$$v^{(\ell)}(\sigma) = (\ell + 1) V_s (1 - (\sigma/a)^2)^\ell H(a - \sigma), \quad \ell = 0, 1, \ldots , \tag{6}$$

and the Gaussian velocity profile

$$v(\sigma; \alpha) = \frac{\alpha V_s}{1 - e^{-\alpha}} e^{-\alpha(\sigma/a)^2} H(a - \sigma), \tag{7}$$

where $H(x)$ is the Heaviside function, i.e., $H(x)=0$, $1/2$, or 1 according as $x$ is negative, zero, or positive. Hence, the velocity profiles in Eqs. (6) and (7) vanish for $\sigma > a$.

The relevance of the Zernike terms $R_{2n}^0$ for the purposes of the present paper is the existence of closed-form formulas, involving spherical Bessel and Hankel functions and Bessel functions of the first kind, respectively, for the on-axis pressure and for the far-field pressure due to a velocity profile described by the term $R_{2n}^0$. Thus, by linearity in Eq. (3), one can compute the on-axis and far-field pressures due to a velocity profile $v$, once its expansion coefficients $u_n$ are available. For instance, the radiators in Eq. (6) give rise to an on-axis pressure expansion in the form of a series of $n+1$ terms $u_\ell j_\ell(kr_-) h_\ell^{(2)}(kr_+)$, with $r_\pm$ argument values directly related to the axial position $(0,0,r)$, while the far-field pressure expansion is a similar series involving terms $u_\ell J_{2\ell+1}(ka \sin\theta)/(ka \sin\theta)$. In the reverse direction, the forward computation schemes for the on-axis and far-field pressures can be complemented by an inverse method with potential use in far-field loudspeaker assessment. Here one estimates the expansion coefficients $u_n$ of a velocity profile $v$ by matching with a measured on-axis pressure data set and then one predicts the far-field sound radiation using the far-field forward formula. Because the on-axis pressure data can be collected in the (relative) near-field of a loudspeaker, this avoids the use of anechoic rooms that would be necessary if the far-field were to be assessed directly. The fact that Zernike series are so efficient in representing velocity profiles is very instrumental here: A smooth velocity profile can already be represented adequately by as few as two to five terms (see Appendix A 2 where this is shown for the truncated Gaussian as an example).

An issue that must be addressed is the following: The set of velocity profiles in Eq. (6) is well known and has been studied in considerable detail, and has in principle the same potential for the purposes of this paper as the set of profiles associated with the Zernike terms. Indeed, closed-form expressions for the far-field pressure due to $v^{(n)}$ were found by Stenzel,[15] and analytical expressions for the on-axis pressure due to the first few $v^{(n)}$ are given by Dekker *et al.*[16] and by Greenspan.[2] However, the formulas for the on-axis pressure in the references given become quite complicated, even for values of $n$ as low as 1 or 2. Furthermore, while Greenspan[2] noted that any polynomial or power series in $(\sigma/a)^2$ can be expanded as a linear combination of the functions $(1 - (\sigma/a)^2)^n$, these expansions require relatively large coefficients due to nearly linear dependence of the expansion functions. Because the Zernike terms are orthogonal, it can be expected that the Zernike expansions behave much better with this respect. Indeed, according to Appendix A, the $n$th coefficient of the expansion into $(1-(\sigma/a)^2)^n$ is roughly a factor $4^n$ larger than the $n$th coefficient in the Zernike expansion [note that the functions $(1-(\sigma/a)^2)^n$ and $R_{2n}^0(\sigma/a)$ have the same mean square value]. This point is of particular importance for the inverse problem, formulated above, of estimating velocity profiles from the on-axis pressure data by matching series representation coefficients. For these two reasons, complicated on-axis pressure expressions and nearly linear dependence, the expansion of velocity profiles in terms of Zernike terms is preferred in this paper.

## II. PAPER OUTLINE

In Sec. III the definition and basic properties of the Zernike terms $R_{2n}^0$ are given, and some of the expansion results that are relevant for this paper are presented. Furthermore, the Hankel transform of $R_{2n}^0$ is presented in closed form. The latter result is of importance both for the forward computation scheme for the far-field and for establishing results on reaction on radiator, radiated power, etc., that are related to King's integral. More information on Zernike expansions is contained in Appendix A.

In Sec. IV the basic formulas for the flat piston are highlighted and discussed. Thus, the closed form involving a spherical Bessel and Hankel function for the on-axis pressure associated with a single term $R_{2n}^0$ is presented, with comments on both near-field and far-field behaviors and on behavior for small and large values of $ka$. Also, in Sec. IV, the far-field expression, in terms of a Bessel function of the first kind, of the pressure associated with a single term $R_{2n}^0$ is presented with particular attention given to the case that $n$ gets large or that $ka$ gets large, etc. In Sec. V the inverse method of estimating the Zernike expansion coefficients of the velocity profile from the on-axis (measured, sampled) pressure data is considered. Together with the forward scheme for computing far-field pressures from Zernike expansions, this yields a loudspeaker assessment method that generalizes a well-known method in audio engineering for estimating the far-field of a loudspeaker from near-field on-axis data in the case of a rigid piston (Keele scheme[17]). In this paper only a few measurements and simulation results will be shown with attention given to more fundamental issues such as the choice of the on-axis sampling scheme and possible ill-posedness of the inversion method.

In Sec. VI the analytic expression for the on-axis pressure developed for the flat piston is extended to dome-shaped radiators. This extension is feasible due to a unique property of the assumed dome profiles, and forms the basis for the characterization of velocity profiles on dome-shaped radiators from on-axis pressure data.

## III. THE ZERNIKE TERMS $R_{2n}^0$

The Zernike terms $R_{2n}^0$ are polynomials of degree $2n$ given by

$$R_{2n}^0(\sigma/a) = P_n(2(\sigma/a)^2 - 1) = \sum_{s=0}^{n} (-1)^s \binom{2n-s}{n} \binom{n}{s} \times (\sigma/a)^{2n-2s}, \tag{8}$$

where $P_n$ is the Legendre polynomial of degree $n$, see Ref. 14 (22.3.8 and 22.5.42). The first few $R_{2n}^0$ are given in Table I, and in Fig. 2 some of them are plotted as a function of $\rho = \sigma/a \in [0,1]$. The $R_{2n}^0$ cannot be interpreted directly in physical terms, unlike the velocity profiles $v^{(\ell)}$ in Eq. (6) in which $\ell$ has the interpretation of a smoothness parameter for the transition from the non-zero values on the piston ($\sigma < a$) to 0 outside the piston ($\sigma > a$). Rather, their significance for loudspeaker analysis stems from the following facts.

TABLE I. Zernike polynomials.

| $n$ | $R_{2n}^0(\sigma/a)$ |
|---|---|
| 0 | 1 |
| 1 | $2(\sigma/a)^2-1$ |
| 2 | $6(\sigma/a)^4-6(\sigma/a)^2+1$ |
| 3 | $20(\sigma/a)^6-30(\sigma/a)^4+12(\sigma/a)^2-1$ |

- They are very efficient and convenient in representing a general velocity profile $v$. This is due to the orthogonality property

$$\int_0^1 R_{2n_1}^0(\rho) R_{2n_2}^0(\rho) \rho d\rho = \frac{\delta_{n_1 n_2}}{2(2n_1+1)} \tag{9}$$

(where $\delta$ is Kronecker's delta), as well as the fact that many velocity profiles considered in loudspeaker analysis can be represented as a Zernike series. In Appendix A, a number of cases are listed, such as the expansion

$$(1-(\sigma/a)^2)^\ell = \sum_{n=0}^{\ell} (-1)^n \frac{2n+1}{n+1} \frac{\binom{\ell}{n}}{\binom{\ell+n+1}{\ell}} R_{2n}^0(\sigma/a), \tag{10}$$

which are relevant for the rigid and simply supported ($\ell = 0,1$) and the clamped radiators ($\ell \geqslant 2$) in Eq. (6), and the expansion

$$e^{-\alpha\sigma^2} = e^{-(1/2)\alpha} \sum_{n=0}^{\infty} (-1)^n (2n+1) \sqrt{\frac{\pi}{\alpha}} I_{n+1/2}(\alpha/2) R_{2n}^0(\sigma/a), \tag{11}$$

which is relevant for the truncated Gaussian radiator in Eq. (7).

- An expansion result of direct relevance to the Rayleigh integral for on-axis field points is the formula

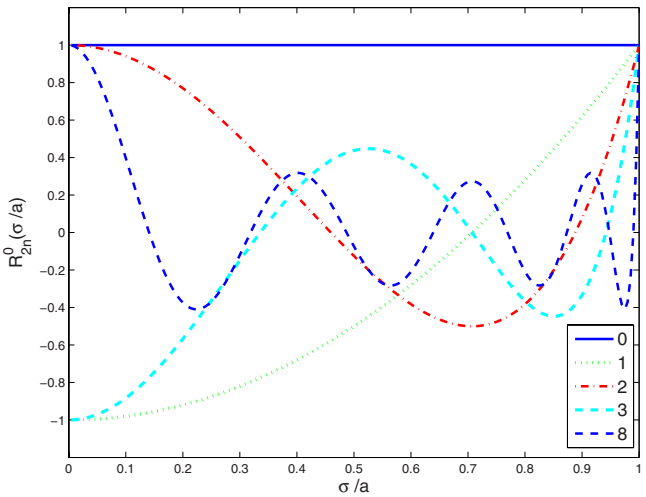


FIG. 2. (Color online) The Zernike terms $R_{2n}^0$ vs $\sigma/a$ for various values of $n$.

$$\frac{e^{-i\lambda(T^2+x\rho^2)^{1/2}}}{-i\lambda(T^2+x\rho^2)^{1/2}} = \sum_{n=0}^{\infty}(2n+1)(-1)^n j_n(\lambda T_-)h_n^{(2)}(\lambda T_+) \times R_{2n}^0(\rho), \tag{12}$$

in which $x \in \mathbb{R}$, $T>0$, $T^2+x>0$, and

$$T_\pm = \tfrac{1}{2}[(T^2+x)^{1/2} \pm T]. \tag{13}$$

This result can be applied to both flat radiators (Sec. IV A) and dome-shaped radiators (Sec. VI). See Appendix A for the proof of Eq. (12) and Sec. IV A for more details on the spherical Bessel functions $j_n$ and spherical Hankel functions $h_n^{(2)}$ occurring in Eq. (12).

- The Hankel transform of zeroth order of the $R_{2n}^0$ has a closed form, viz.,

$$\int_0^a J_0(u\sigma)R_{2n}^0(\sigma)\sigma d\sigma = (-1)^n \frac{a}{u}J_{2n+1}(ua). \tag{14}$$

This formula has been proved in Ref. 7 as a special case of a formula expressing the $m$th order Hankel transform of Zernike polynomials of azimuthal order $m$ in terms of Bessel functions of the first kind. This formula is very important for the development of explicit analytic results in the spirit of Ref. 2. For the purposes of the present paper, the result is important since it gives the far-field expression for the pressure due to a single term $R_{2n}^0$ in the velocity profile, see Sec. IV B and Appendix B.

## IV. ON-AXIS AND FAR-FIELD EXPRESSIONS FOR THE FLAT PISTON

The velocity profile $v(\sigma)$ considered in this section (normal component) vanishes outside the disk $\sigma \leqslant a$ and has been developed into a Zernike series as in Eq. (3) with coefficients $u_n$ given in accordance with Eq. (5) or explicitly as in the cases discussed earlier.

### A. On-axis expression

There holds for an on-axis point $\underline{r}=(0,0,r)$ with $r \geqslant 0$ by radial symmetry of the integrand in Eq. (1) the formula

$$p(\underline{r}) = i\rho_0 ck \int_0^a v(\sigma)\frac{e^{-ik(r^2+\sigma^2)^{1/2}}}{(r^2+\sigma^2)^{1/2}}\sigma d\sigma. \tag{15}$$

Inserting $v(\sigma)=V_s\Sigma_{n=0}^{\infty}u_nR_{2n}^0(\sigma/a)$ into the integral and setting $\sigma=a\rho$, $0 \leqslant \rho \leqslant 1$, it follows that

$$p(\underline{r}) = i\rho_0 cka^2V_s\sum_{n=0}^{\infty}u_n\int_0^1 \frac{e^{-ik(r^2+a^2\rho^2)^{1/2}}}{(r^2+a^2\rho^2)^{1/2}}R_{2n}^0(\rho)\rho d\rho. \tag{16}$$

Then by Eq. (12) and orthogonality of the Zernike terms,

$$p(\underline{r}) = \frac{1}{2}\rho_0 cV_s(ka)^2\sum_{n=0}^{\infty}\gamma_n(k,r)u_n, \tag{17}$$

in which

$$\gamma_n(k,r) = (-1)^n j_n(kr_-)h_n^{(2)}(kr_+),$$

$$r_\pm = \tfrac{1}{2}(\sqrt{r^2+a^2} \pm r). \tag{18}$$

The $j_n$ and $h_n^{(2)}=j_n-iy_n$ are the spherical Bessel and Hankel functions, respectively, of the order $n=0,1,\ldots$, see Ref. 14 (Sec. 10.1). In particular, $j_0(z)=(\sin z)/z$ and $h_0^{(2)}(z)=(ie^{-iz})/z$.

What follows now is a discussion of the results in Eqs. (17) and (18). The $r_\pm$ of Eq. (18) satisfy

$$0 \leq r_- \leq \tfrac{1}{2}a \leq r_+, \quad r_+r_- = \tfrac{1}{4}a^2, \quad r_+ + r_- = \sqrt{r^2+a^2}. \tag{19}$$

Consider the case of the rigid piston, i.e., $\ell=0$ in Eq. (10). Then $u_0=1$, $u_1=u_2=\cdots=0$, and from Eqs. (17)–(19) it is found, using $j_0(z)=\sin z/z$ and $h_0^{(2)}(z)=ie^{-iz}/z$ and some administration, that

$$p(\underline{r}) = \frac{1}{2}\rho_0 cV_s(ka)^2\frac{\sin kr_-}{kr_-}\frac{ie^{-ikr_+}}{kr_+} = 2i\rho_0 cV_s e^{-(1/2)ik((r^2+a^2)^{1/2}+r)}\sin\frac{1}{2}k((r^2+a^2)^{1/2}-r). \tag{20}$$

This is the classical result on the on-axis pressure for a rigid piston as can be found in the textbooks, see, e.g., Ref. 11 [Eqs. (8.31a) and (8.31b)]. Figure 3 shows a plot of $|\gamma_{\ell=n=0}(k,r)|$ as a function of $r/a$ (rigid piston) and of $|\gamma_n(k,r)|$ for $n=1,2,3$. Some comments on these plots are presented at the end of this subsection.

For the simply supported radiator, case $\ell=1$ in Eq. (6), one has $u_0=1$ and $u_1=-1$ so that

$$p(\underline{r}) = \tfrac{1}{2}\rho_0 cV_s(ka)^2[j_0(kr_-)h_0^{(2)}(kr_+) + j_1(kr_-)h_1^{(2)}(kr_+)], \tag{21}$$

and for the lowest order clamped radiator, case $\ell=2$ in Eq. (6), one has $u_0=1$, $u_1=-3/2$, and $u_2=1/2$, so that

$$p(\underline{r}) = \tfrac{1}{2}\rho_0 cV_s(ka)^2\left[j_0(kr_-)h_0^{(2)}(kr_+) + \tfrac{3}{2}j_1(kr_-)h_1^{(2)}(kr_+) + \tfrac{1}{2}j_2(kr_-)h_2^{(2)}(kr_+)\right]. \tag{22}$$

The results of Eqs. (21) and (22) generalize to higher $\ell$ immediately since the required coefficients $u$ for the general case are available through Eq. (10). Also see Ref. 6, Eqs. (9)–(11), where the expression for $\ell=1,2$ leads to considerable complications. In Fig. 4 the rigid piston ($\ell=0$), the simply supported radiator ($\ell=1$), and the first two clamped radiators ($\ell=2,3$) are considered ($|p(\underline{r})|$, normalized as a function of $r/a$).

The next comments concern the behavior of the terms $\gamma_n$ in Eq. (18). From Eqs. (18) and (19) it follows that

$$r_- \approx \tfrac{1}{2}(a-r) \approx \tfrac{1}{2}a \approx \tfrac{1}{2}(a+r) \approx r_+, \quad r \ll a. \tag{23}$$

Therefore, when $ka$ is large and $r \to 0$ (with $n$ not large), it follows from the results in Ref. 14, Sec. 10.1 that

$$|\gamma_n(k,r)| \approx \frac{|\cos\frac{1}{2}k(a-r)|}{\frac{1}{4}k^2a^2}, \tag{24}$$

confirming the presence of zeros and the largely $n$-independent envelope of the curves in Fig. 3 near $r=0$.

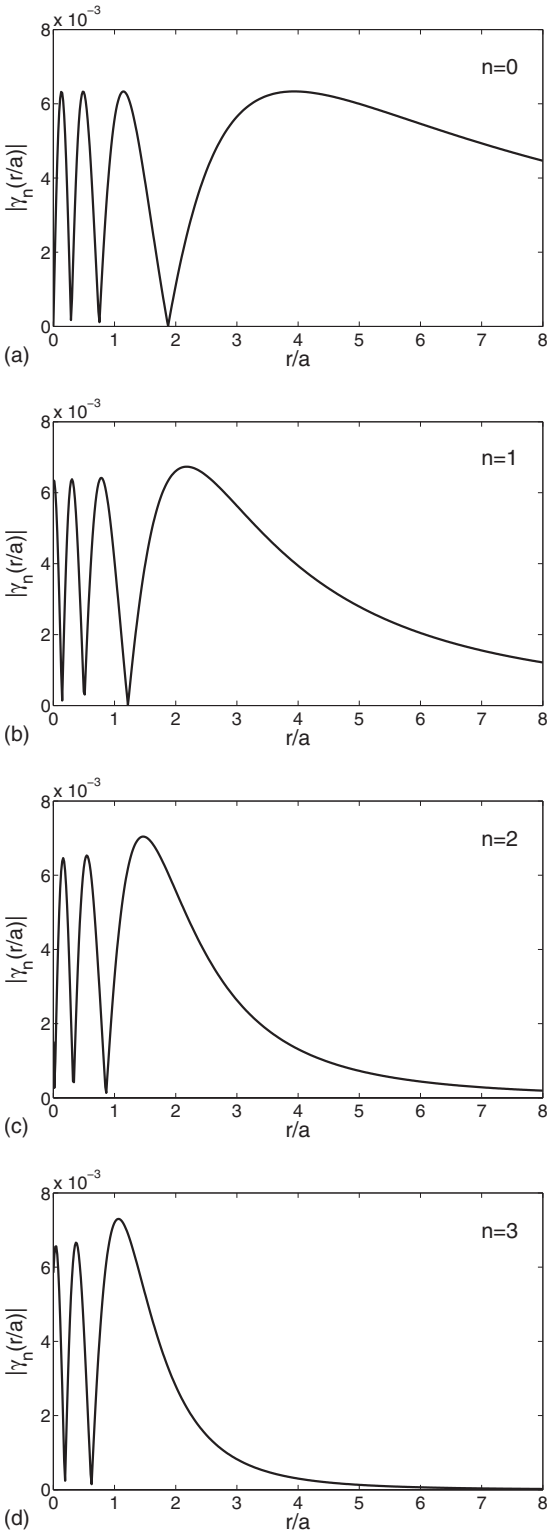


FIG. 3. The product $|j_n(kr_-)h_n^{(2)}(kr_+)|$ from Eq. (18), for $n=0,\ldots,3$, vs $r/a$, where $a/\lambda=4$ and $a=0.1$ m, which yields $f=13.7$ kHz and $ka=8\pi$. (a) $n=0$, (b) $n=1$, (c) $n=2$, and (d) $n=3$.

Finally, when $r \gg a$, it follows from Eqs. (18) and (19) that

$$r_- \approx \frac{a^2}{4r}, \quad r_+ \approx r. \tag{25}$$

Therefore, from Ref. 14, Sec. 10.1,

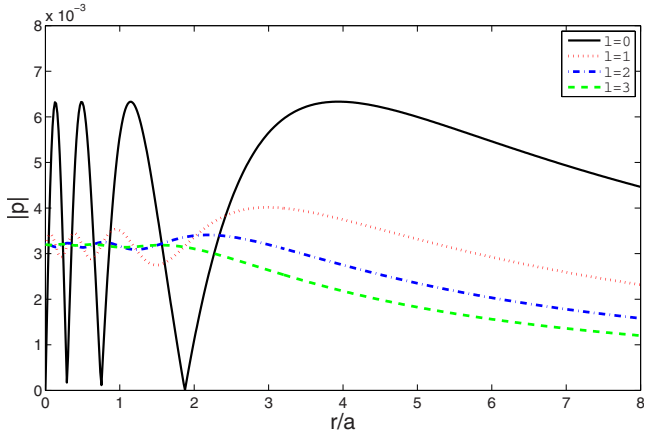


FIG. 4. (Color online) Normalized $|p|$ vs $r/a$ for the rigid piston ($\ell=0$) (solid curve), the simply supported radiator ($\ell=1$) (dotted curve), and the first two clamped radiators ($\ell=2,3$) (dashed-dotted and dashed curves, respectively) using Eq. (17). Here $a/\lambda=4$ and $ka=8\pi$. The normalization is equal to $(\ell+1)/2\rho_0 c V_s (ka)^2$. The factor $\ell+1$ allows an easier comparison of the four curves.

$$\gamma_n(k,r) \approx \frac{\left(\frac{-ika^2}{4r}\right)^n}{1\times 3\cdots(2n+1)} \frac{e^{-ikr_+}}{-ikr_+}, \tag{26}$$

which shows an $O(1/r^{n+1})$-behavior of $\gamma_n(k,r)$ as $n\to\infty$.

### B. Far-field expression

Using the Zernike expansion (3) of $v(\sigma)$ it is shown in Appendix B that the following far-field approximation holds: When $\underline{r}=(r\sin\theta, 0, r\cos\theta)$ and $r\to\infty$,

$$p(\underline{r}) \approx i\rho_0 ckV_s \frac{e^{-ikr}}{r} a^2 \sum_{n=0}^{\infty} u_n (-1)^n \frac{J_{2n+1}(ka\sin\theta)}{ka\sin\theta}. \tag{27}$$

The result of Eq. (27) will now be discussed. In the case of a rigid piston, it follows that

$$p(\underline{r}) \approx i\rho_0 ckaV_s \frac{e^{-ikr}}{r} \frac{J_1(ka\sin\theta)}{ka\sin\theta}. \tag{28}$$

This is the familiar result for the far-field pressure of a rigid piston as can be found in the textbooks, see, e.g., Ref. 11 [Eq. (8.35)]. In Fig. 5 a plot can be found of $|J_{2n+1}(ka\sin\theta)/ka\sin\theta|$, $n=0,1,2,3$.

For the simply supported radiator, case $\ell=1$ in Eq. (6), and for the clamped radiators, cases $\ell\geqslant 2$ in Eq. (6), there is the far-field result of Stenzel,[15]

$$p(\underline{r}) \approx i\rho_0 cV_s ka^2(\ell+1)!2^\ell \frac{e^{-ikr}}{r} \frac{J_{\ell+1}(ka\sin\theta)}{(ka\sin\theta)^{\ell+1}}; \tag{29}$$

also see Ref. 2 (Sec. II).

Alternatively, the coefficients $u$ in the Zernike expansion of the $v^{(\ell)}$ in Eq. (6) are available per Eq. (10), and this gives the far-field approximation of $p(\underline{r})$ via Eq. (27) in a form different from Eq. (29). Equating the $r$-independent parts of the right-hand sides ( RHSs) of the two expressions leads to a non-obvious analytic relation between Bessel functions,

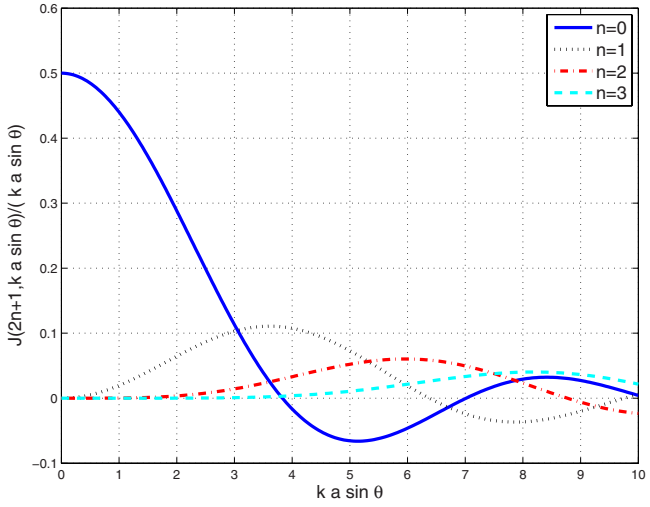


FIG. 5. (Color online) $|J_{2n+1}(ka\sin\theta)/ka\sin\theta|$ vs $ka\sin\theta$.

$$\ell!2^{\ell}\frac{J_{\ell+1}(x)}{x^{\ell+1}}=\sum_{n=0}^{\ell}\frac{2n+1}{n+1}\frac{\binom{\ell}{n}}{\binom{\ell+n+1}{\ell}}\frac{J_{2n+1}(x)}{x}, \tag{30}$$

and either method yields the result shown in Fig. 6.

Some comments on the behavior of the terms $J_{2n+1}(z)/z$, $z=ka\sin\theta$, as they occur in the series in Eq. (27) are presented now. From the asymptotics of the Bessel functions, as given in Ref. 14 [Eq. (9.3.1)], it is seen that in the series in Eq. (27) only those terms contribute significantly for which $2n+1\leqslant\frac{1}{2}e\,ka\sin\theta$. In particular, when $\theta=0$, it is only the term with $n=0$ that is non-vanishing, and this yields

$$p((0,0,r))\approx\frac{1}{2}i\rho_0cV_ska^2\frac{e^{-ikr}}{r},\quad r\to\infty. \tag{31}$$

This is in agreement with what is found from Eq. (17) when only the term with $n=0$ is retained and $r_+$ is replaced with $r$, and $r_-$ is replaced with 0. For small values of $ka$ the terms in the series (27) decay very rapidly with $n$. For large values of $ka$, however, a significant number of terms may contribute, especially for angles $\theta$ far from 0.

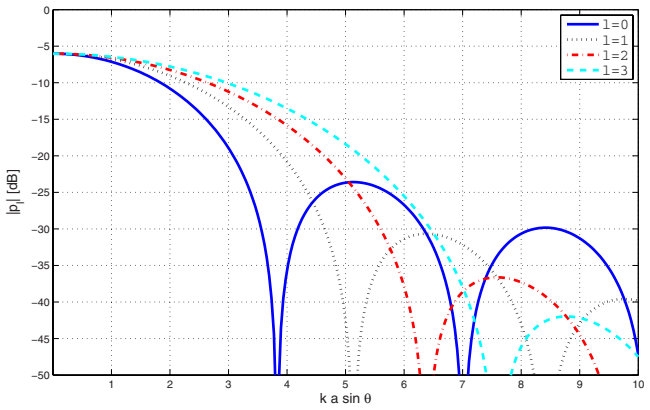


FIG. 6. (Color online) Normalized $|p|$ vs $ka\sin\theta$, using the Zernike expansion of the $v^{(\ell)}$ and Eq. (27) or Eq. (29).

## V. ESTIMATING VELOCITY PROFILES FROM ON-AXIS RADIATION DATA FOR FAR-FIELD LOUDSPEAKER ASSESSMENT

### A. Estimating velocity profiles from on-axis radiation

The on-axis expressions (17) and (18) for the pressure can, in reverse direction, be used to estimate the velocity profile on the disk from (measured) on-axis data via its expansion coefficients $u_n$. This can be effectuated by adopting a matching approach in which the coefficients $u_n$ in the "theoretical" expressions (17) and (18) are determined so as to optimize the match with at $M+1$ points measured data. Thus, one has for the pressure $p_m=p((0,0,r_m))$ due to the velocity profile $v(\sigma)=V_s\Sigma_{n=0}^{N}u_nR_{2n}^0(\sigma/a)$ the expression

$$p_m=\frac{1}{2}\rho_0cV_s(ka)^2\sum_{n=0}^{N}(-1)^nj_n(kr_{m,-})h_n^{(2)}(kr_{m,+})u_n, \tag{32}$$

where $r_m\geqslant 0$ and

$$r_{m,\pm}=\tfrac{1}{2}(\sqrt{r_m^2+a^2}\pm r_m), \tag{33}$$

and $m=0,1,\ldots,M$. With

$$A=(A_{mn})_{\substack{m=0,1,\ldots,M,\\ n=0,1,\ldots,N}},$$

$$A_{mn}=\tfrac{1}{2}\rho_0cV_s(ka)^2j_n(kr_{m,-})h_n^{(2)}(kr_{m,+}), \tag{34}$$

$$\underline{p}=[p_0,\ldots,p_M]^T,\quad \underline{u}=[u_0,\ldots,u_N]^T, \tag{35}$$

the relation between on-axis pressures $p_m$ and coefficients $u_n$ can be concisely written as

$$A\underline{u}=\underline{p}. \tag{36}$$

Now given a (noisy) on-axis data vector $\underline{p}$ one can estimate the coefficients' vector $\underline{u}$ by adopting a least mean-squares approach for the error $A\underline{u}-\underline{p}$. This will be illustrated by a simulated experiment and, subsequently, by a real experiment, below. In the simulated experiment, we assume a loudspeaker with a Gaussian velocity profile ($\alpha=2$), as shown in Fig. 7(a) curve $v_G$ (dashed-dotted) and given by the left-hand side (LHS) of Eq. (A2). This profile is approximated using three Zernike coefficients ($u_0=0.4323$, $u_1=-0.4060$, and $u_2=0.1316$) given by the RHS of Eq. (A2), and this leads to the velocity profile $v_a$ (solid curve) in Fig. 7(a). It can be seen from Fig. 7(a) that including three Zernike terms provides a fair approximation ($3\times10^{-2}$ absolute accuracy on the whole range). Using the three coefficients of the approximated velocity profile, the sound pressure was calculated by applying Eq. (17) and plotted in Fig. 7(b) as $p_{\text{calc}}$ (solid curve). Then random white noise was added to $p_{\text{calc}}$ as shown as $p$ +noise in Fig. 7(b) (dotted curve). Subsequently the inversion procedure was followed by using the noisy pressure data vector $\underline{p}$ to estimate the coefficients' vector $\underline{u}$ by adopting a least mean-squares approach for the error $A\underline{u}-\underline{p}$ [see Eq. (36)]. Using the recovered three Zernike coefficients the velocity profile and pressure data were calculated and plotted in Fig. 7(a) (thick dotted curve) and Fig. 7(b) (thick dotted curve), respectively. It appears that the inversion procedure is rather robust against noise since the calculated and recovered pressure curves in Fig. 7(b) are almost coincident.

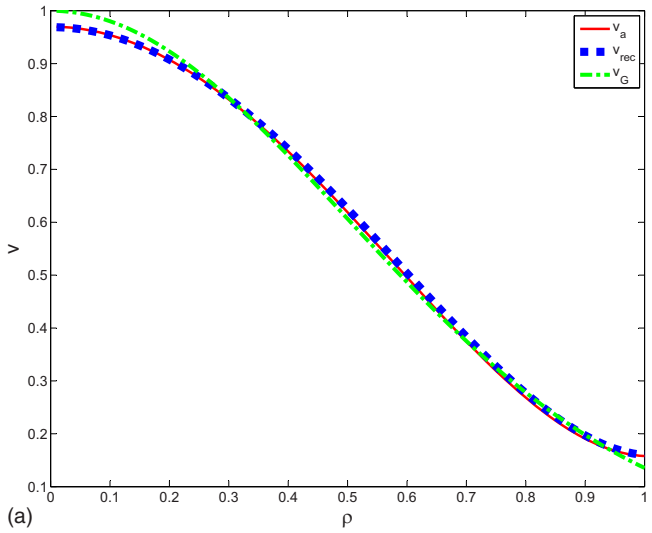


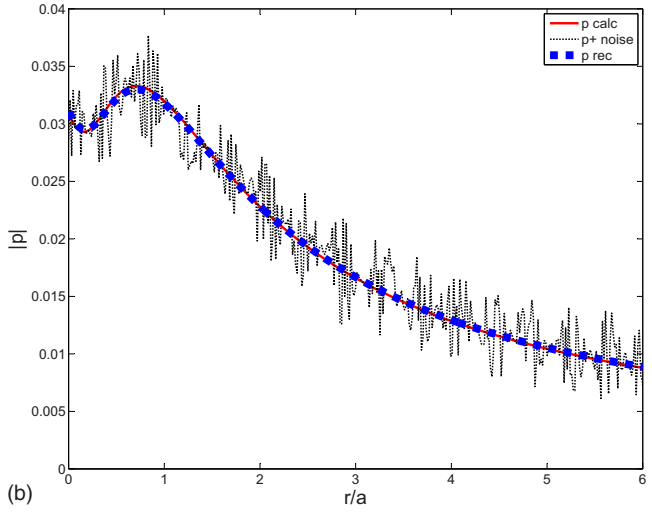


FIG. 7. (Color online) Simulated experiment. (a) Gaussian velocity profile ($\alpha=2$) $v_G$ vs $\rho$ [dashed-dotted curve, given by the LHS of Eq. (A2)]. Approximated velocity profile $v_a$ using the series at the RHS of Eq. (A2), truncated at $n=2$ (solid curve). From noisy pressure data recovered velocity profile $v_{\mathrm{rec}}$ (thick dotted curve). (b) Sound pressure using Eq. (17) and $ka=8$ ($p_{\mathrm{calc}}$, solid curve). Pressure with added noise ($p+$noise, dotted curve). Recovered pressure data ($p_{\mathrm{rec}}$, thick dotted curve).

For the second experiment we measured a loudspeaker (vifa MG10SD09-08, $a=3.2$ cm) in an IEC-baffle,[18] at ten near-field positions ($\underline{r}_m=0.00,0.01,0.02,0.03,0.04,0.05,0.07,0.10,0.13,0.19$ m), and finally in the far-field at 1 m distance at 13.72 kHz ($ka=8.0423$). The magnitude of the sound pressure is plotted in Fig. 8 (solid curve, "$p$ meas"). Using the same procedure as described above for the first experiment, the inverse process was followed by using the ten measured near-field pressure data points to estimate the coefficients' vector $\underline{u}$. Using four Zernike coefficients the pressure data were recovered and plotted in Fig. 8 (dotted curve, "$p$ rec"). It appears that the two curves show good resemblance to each other and that only four coefficients are needed to provide a very good description of the near-field at rather high frequencies (13.72 kHz). Furthermore, it appears that using these four coefficients, the calculated sound pressure level at 1-m distance yields −42 dB. The measured value at that far-field point is −44 dB. These values match

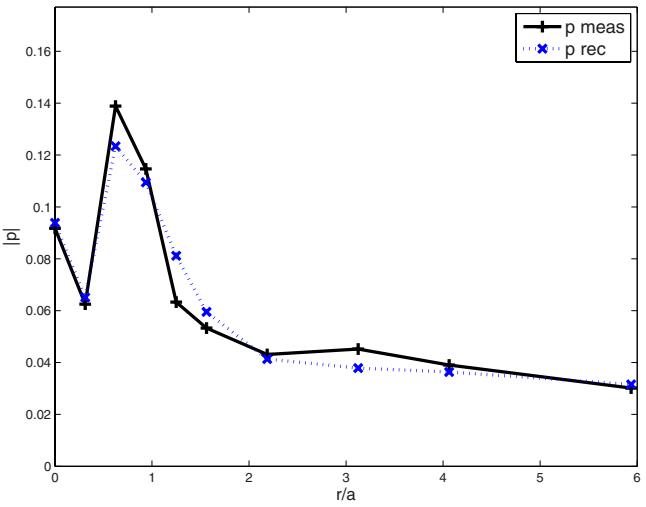


FIG. 8. (Color online) Measured loudspeaker at 13.72 kHz ($ka=8.0423$, $p$ meas, solid curve) vs $r/a$. Recovered pressure data ($p$ rec, dotted curve).

rather closely, even though at the used frequency of 13.72 kHz the cone vibrates not fully circularly symmetric anymore due to break-up behavior. This match provides a proof of principle as the far-field measurement point was not used to determine the Zernike coefficients, also see Sec. V B below.

In the experiments just described, no particular effort was spent in forming and handling the linear systems so as to have small condition numbers. The condition number, the ratio of the largest and smallest non-zero singular value of the matrix $A$ in Eq. (34), equals 50 in the case of the loudspeaker experiment leading to Fig. 8. In Fig. 9 the condition number is plotted as a function of the number $N+1$ of columns for the case of the simulation experiment leading to Fig. 7. It is seen that the condition number grows rapidly with $N$. It is expected that considerably improved condition numbers result when the structure of the linear systems and their constituent functions $j$ and $h$ is employed; this is, however, outside the scope of the present paper. The influence of the condition number on noise-sensitivity and the like of the

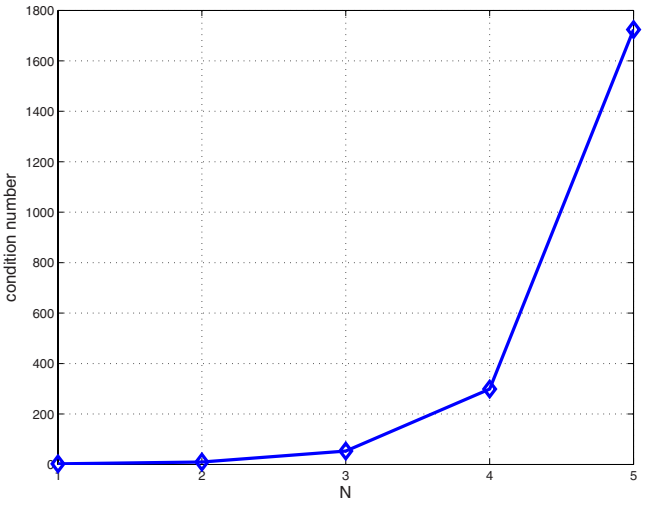


FIG. 9. (Color online) The condition numbers of the first experiment (diamonds, for $ka=8$, $\alpha=2$, and $M=500$).

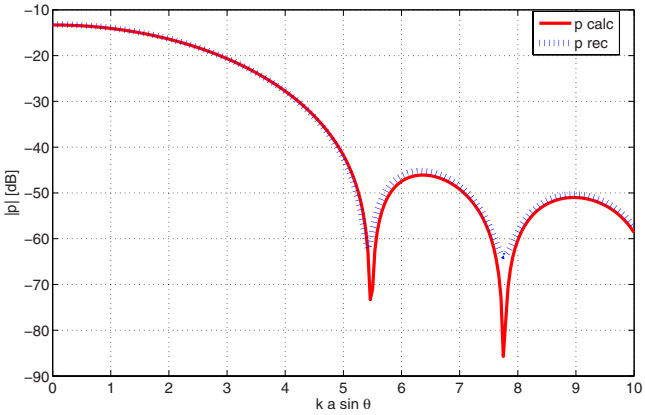


FIG. 10. (Color online) Simulated experiment Gaussian radiator ($\alpha=2$). Normalized sound pressure in the far-field using Eq. (27) and $ka=8$ ($p_{\text{calc}}$, solid curve). Recovered normalized far-field pressure data ($p_{\text{rec}}$, dotted curve).

solution of least-squares problems is discussed in Ref. 19. In practical cases the number of required Zernike coefficients will be less than, say, six. This will not cause numerical difficulties. Furthermore, such a modest number of coefficients already allow a large set of velocity profiles.

### B. Far-field assessment from on-axis measurements

In Ref. 17 a method is described to assess low-frequency loudspeaker performance in the on-axis far-field from an on-axis near-field measurement. In the case of the rigid piston, the on-axis pressure $p(\underline{r})=p((0,0,r))$ is given by Eq. (20). Now assume $ka \ll 1$. When $r \ll a$ it holds that

$$\sin\left(\tfrac{1}{2}k\sqrt{r^2+a^2}-r\right) \approx \sin\left(\tfrac{1}{2}ka\right) \approx \tfrac{1}{2}ka, \tag{37}$$

and, when $r \gg a$ it holds that

$$\sin\frac{1}{2}k(\sqrt{r^2+a^2}-r) \approx \sin\left(\frac{ka^2}{4r}\right) \approx \frac{ka^2}{4r}. \tag{38}$$

Therefore, the ratio of the moduli of near-field and far-field on-axis pressures is given by $2r/a$. This is the basis of Keele's method;[17] it allows far-field loudspeaker assessment without having to use an anechoic room.

With the inversion procedure to estimate velocity profiles from on-axis data (which are taken in the relative near-field) as described in Sec. V A together with the forward calculation scheme for the far-field as described in Sec. IV B, it is now possible to generalize Keele's scheme.[17] This is illustrated by comparing the far-field responses pertaining to the two sets of Zernike coefficients occurring in the Gaussian simulated experiment, see Fig. 7 in Sec. V A. Using Eq. (27) the normalized far-field pressure is plotted in Fig. 10 as $p_{\text{calc}}$ (solid curve) and $p_{\text{rec}}$ (dotted) curves, respectively ($\alpha=2$ and $ka=8$), where the normalization is such that the factor in front of the series at the RHS of Eq. (27) equals unity. It appears that the two curves are very similar. This confirms that the $u_n$ obtained from the noisy near-field measured pressure data yield a good estimate of the far-field spatial pressure response.

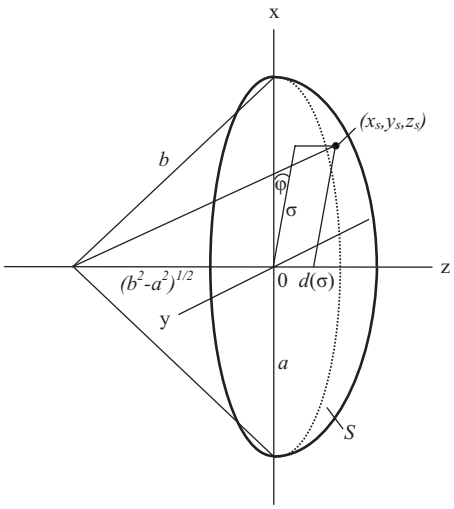


FIG. 11. Geometry of a (convex) dome-shaped radiator, with radiating surface $S$ given as the set of points $(x_s,y_s,z_s)=(\sigma\cos\varphi,\sigma\sin c,d(\sigma))$ in accordance with Eqs. (39) and (40).

## VI. GENERALIZATION OF THE ON-AXIS RESULT TO DOME-SHAPED RADIATORS

The on-axis result in Eq. (17) for the flat-piston radiators is now generalized to dome-shaped and inverted-dome-shaped radiators. The formal treatment of the dome-shaped radiators requires solving the Helmholtz equation. However, in this paper, a geometrical approach is used, where the Rayleigh integral in Eq. (1) is maintained, with distance function $r'$ defined in accordance with the function $d$ describing the dome surface. This geometrical approach is similar to the one used by Bordoni[20] and Kates.[21] From Suzuki and Tichy[22] (Sec. 2 A) it appears that the geometrical approach yields a fairly good approximation, at least, in the high-frequency region.

Thus the considered radiating surface $S$ is now assumed to consist of the points

$$\underline{r}_s = (x_x,y_s,z_s) = (\sigma\cos\varphi,\sigma\sin\varphi,d(\sigma)),$$

$$0 \le \sigma \le a, \quad 0 \le \varphi \le 2\pi, \tag{39}$$

in which $d(\sigma)$ is the function

$$d(\sigma) = \pm[(b^2-\sigma^2)^{1/2}-(b^2-a^2)^{1/2}], \quad 0 \le \sigma \le a, \tag{40}$$

with $b \geqslant a$. The $+$-sign in Eq. (40) corresponds to a convex dome while the $-$-sign corresponds to a concave (or inverted) dome. In the $+$-case, $S$ is the cap of a sphere of radius $b$ bounded by the parallel of latitude of angle arccos $(a/b)$. In Fig. 11 the situation is depicted for a convex dome. Thus the dome surface $S$ consists of a spherical cap whose boundary coincides with the boundary of the infinite baffle.

The integral expression for the pressure is still given by the Rayleigh integral in Eq. (1), with $v(\underline{r}_s)$ the normal component of the velocity distribution on $S$. The normal on the surface $S$ is given by

$$\underline{n}(\sigma) = \frac{1}{b}(\pm\sigma\cos\varphi,\ \pm\sigma\sin\varphi,(b^2-\sigma^2)^{1/2}). \tag{41}$$

The function $r'$, being the distance between a field point $\underline{r} = (r\sin\theta, 0, r\cos\theta)$ and the point $\underline{r}_s$ in Eq. (39), is given by

$$r' = (r^2+\sigma^2-2r\sigma\sin\theta\cos\varphi - 2rd(\sigma)\cos\theta + d^2(\sigma))^{1/2}, \tag{42}$$

and is to be considered in the set $(r,\theta)$ with $r\cos\theta \geqslant d(\sigma)$.

When transforming the Rayleigh integral (1) from an integral over the disk $\sigma \leqslant a$, one should account for the surface element in the usual manner according to

$$dS = \sqrt{1+\left(\frac{\partial f}{\partial x}\right)^2+\left(\frac{\partial f}{\partial y}\right)^2}\,dxdy = \frac{b\sigma d\sigma d\varphi}{\sqrt{b^2-\sigma^2}}, \tag{43}$$

where $f(x,y)=d(\sqrt{x^2+y^2})$. Then writing

$$v(\sigma) = v((\sigma\cos\varphi, \sigma\sin\varphi, d(\sigma))), \quad 0 \leq \sigma \leq a, \tag{44}$$

one obtains

$$p(\underline{r}) = \frac{i\rho_0 ck}{2\pi}\int_0^a\int_0^{2\pi} v(\sigma)\frac{e^{-ikr'}}{r'}\frac{b}{\sqrt{b^2-\sigma^2}}\sigma d\sigma d\varphi. \tag{45}$$

In Appendix C the following is shown. Let

$$g(\tau) = \tau\left(\frac{2-(1-c_0)\tau^2}{1+c_0}\right)^{1/2}, \tag{46}$$

in which $c_0=\sqrt{1-(a/b)^2}$. Then $g$ is a mapping from $[0, 1]$ onto $[0, 1]$. Now when

$$W(\tau) = v(ag(\tau)), \quad W(\tau) = W_s\sum_{n=0}^{\infty} w_n R_{2n}^0(\tau), \tag{47}$$

with $W_s$ such that $w_0=1$, then

$$p(\underline{r}) = i\rho_0 cW_s(ka)^2\frac{1}{1+c_0}\sum_{n=0}^{\infty}\delta_n(k,r)w_n, \tag{48}$$

where

$$\delta(k,r) = (-1)^n j_n\left(k\left(r_- + \tfrac{1}{2}d(0)\right)\right)h_n^{(2)}\left(k\left(r_+ + \tfrac{1}{2}d(0)\right)\right). \tag{49}$$

Here $r_\pm$ is as in Eqs. (17) and (18). The validity of this result is largely due to the special form of the assumed dome shape and does not seem to admit a generalization to other dome shapes.

A discussion of the result of Eqs. (47)–(49) follows now. As Eq. (47) shows, a simple warping operation on $v$ is required so as to obtain the series representation (48) with coefficients per Eq. (49) that is strikingly similar to the result of Eqs. (17) and (18). In Fig. 12 the warping function $g(\tau)$, $0 \leqslant \tau \leqslant 1$, for $s_0=a/b=1, 0.9, 0.5, 0$ is shown, the case $s_0=0$ yielding $g(\tau)=\tau$ [i.e., the result of Eqs. (17) and (18)]. The plots show that for moderate values of $s_0$, say, $s_0 \leqslant 1/2$, the influence of the warping operation is quite modest. Consequently, in that case, $w_n \approx u_n$, where $u_n$ are the coefficients in the Zernike expansion (3) of $v$ itself.

A particularly interesting case occurs when $b=a$ so that $S$ is a hemisphere. Then $c_0=0$ and

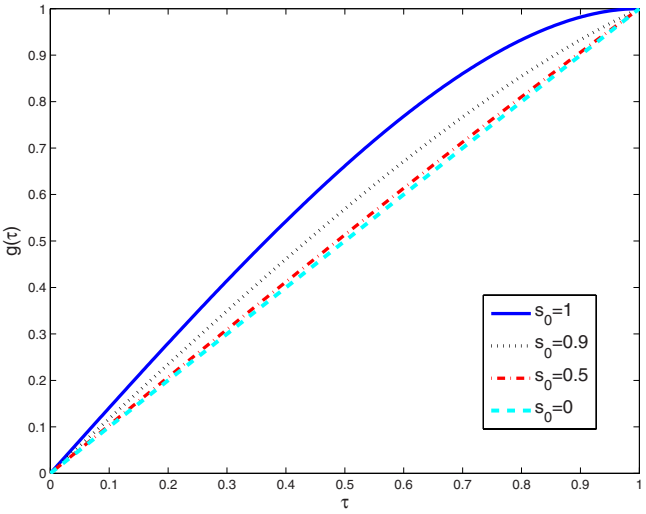


FIG. 12. (Color online) The warping function [Eq. (46)] $g(\tau)$ vs $\tau$.

$$g(\tau) = \tau(2-\tau^2)^{1/2} = (1-(1-\tau^2)^2)^{1/2}. \tag{50}$$

When $v(\sigma)=v^{(\ell)}(\sigma)=(\ell+1)V_s(1+(\sigma/a)^2)^\ell$, see Eq. (6), one gets

$$v^{(\ell)}(ag(\tau)) = (\ell+1)V_s(1-\tau^2)^{2\ell} = \frac{\ell+1}{2\ell+1}v^{(2\ell)}(\tau), \tag{51}$$

and so the required Zernike coefficients $w_n$ in Eq. (47) are available per Appendix A 1, case $k=2\ell$. For the Gaussian in Eq. (7) one computes, using Eq. (50) and $\exp(x)=\Sigma_{\ell=0}^{\infty}x^\ell/l!$,

$$v(ag(\tau);\alpha) = \frac{\alpha V_s}{e^\alpha-1}\sum_{\ell=0}^{\infty}\frac{\alpha^\ell}{\ell!}(1-\tau^2)^{2\ell}. \tag{52}$$

Hence the required Zernike coefficients $w_n$ in Eq. (47) can be obtained explicitly in the form of infinite series by combining Eq. (7) and Appendix A 1.

## VII. DISCUSSION AND OUTLOOK

In this paper the foundation is laid for a method to perform forward and inverse sound pressure computations for circular radiators with a non-uniform velocity profile. In the forward problem, the velocity profile is assumed to be known and the on-axis and far-field sound pressures are expressed analytically in terms of Zernike expansion coefficients of the velocity profile and (spherical) Bessel (and Hankel) functions. In the inverse problem, the velocity profile is unknown and is estimated in terms of Zernike expansion coefficients from on-axis pressure data by adopting a matching approach based on the analytic result for the on-axis pressure. Well-behaved velocity profiles are already adequately represented by only a few terms of their Zernike expansion. Therefore, the Zernike series approach is more convenient for both the forward problems and the inverse problem than, for instance, an approach based on expansions involving the family of rigid, simply supported, and clamped radiators. The forward and inverse methods are proposed for use in assessment of the far-field of a loudspeaker without the need for an anechoic room. Here, the Zernike coefficients of the velocity profile are estimated from the on-axis (rela-

tively near-field) data, and these coefficients are used in the forward scheme to compute the far-field. This assessment procedure has not been fully worked out in the present paper due to a variety of practical issues that need to be addressed. Among these practical issues are

- choice of the on-axis measurement points,
- condition of the linear systems that arise,
- influence of $ka$,
- influence of noise,
- influence of misalignment of the measurement points,
- influence of inclination of the measurement axis, and
- incorrect setting of the radius of the radiator,

while various combinations of these issues should also be considered. The authors intend to work out the method for the loudspeaker assessment with attention for the above mentioned points.

In this paper, the theory has been developed mainly for flat radiators. However, the basic result for the on-axis pressure as a series expansion, in terms of Zernike coefficients and spherical Bessel and Hankel functions, has been generalized to the case of dome-shaped radiators. It is, therefore, to be expected that both the forward and the inverse methods can also be generalized to the case of dome-shaped radiators. The forward problem and the inverse problem concerning the on-axis pressure are not much more difficult than in the case of flat radiators: Only a simple warping operation performed on the velocity profile is required. The computation of the far-field is, however, more complicated for the dome-shaped radiators. In the first place, the estimated Zernike coefficients require a transformation due to the warping operation. Secondly, the basic integrals corresponding to a single Zernike term, which occur in the far-field expression for the sound pressure, are not readily expressed in Bessel functions as was the case for flat radiators. The authors intend to develop the method both on a theoretical and practical level for dome-shaped radiators as well.

## VIII. CONCLUSIONS

Zernike polynomials are an efficient and robust method to describe velocity profiles of resilient sound radiators. Only a few coefficients are necessary to approximate a wide variety of velocity profiles including the rigid piston, the simply supported radiator, the clamped radiators, Gaussian radiators, as well as real loudspeaker drivers. This method enables one to solve the inverse problem of calculating the actual velocity profile of the radiator using (measured) on-axis sound pressure data. This computed velocity profile allows the extrapolation to far-field loudspeaker pressure data, including off-axis behavior. The forward computation scheme can be extended to dome-shaped radiators with arbitrary velocity distributions.

## APPENDIX A: ZERNIKE EXPANSIONS

In this appendix a number of explicit Zernike expansions for the radially symmetric case are collected, some general results on Zernike expansions are given, and some examples are given to demonstrate that the $n$th coefficient in a Zernike expansion is roughly $4^n$ as small as the $n$th coefficient in an expansion based on the functions $(1-(\sigma/a)^2)^n$ in Eq. (6). The results are presented in terms of the normalized variable $\rho=\sigma/a$, $0\leqslant\rho\leqslant 1$.

### 1. Zernike expansion of $\rho^{2\ell}$, $(1-\rho^2)^\ell$

From Ref. 23, Appendix A,

$$\rho^{2\ell}=\sum_{n=0}^{\ell}\frac{2n+1}{n+1}\frac{\binom{\ell}{n}}{\binom{\ell+n+1}{\ell}}R_{2n}^0(\rho). \tag{A1}$$

Using $P_n(-x)=(-1)^nP_n(x)$, so that $R_{2n}^0((1-\rho)^2)^{1/2})=(-1)^nR_{2n}^0(\rho)$, one obtains Eq. (10).

### 2. Expansion of $e^{-\alpha\rho^2}$

It holds that

$$e^{-\alpha\rho^2}=e^{-(1/2)\alpha}\sum_{n=0}^{\infty}(-1)^n(2n+1)\sqrt{\frac{\pi}{\alpha}}I_{n+1/2}(\alpha/2)R_{2n}^0(\rho), \tag{A2}$$

where $(\pi/2z)^{1/2}I_{n+1/2}(z)$ is the modified spherical Bessel function of order $n$. See Ref. 14, Secs. 10.2 and 10.2.37, with $z=\alpha/2$ and $\cos\theta=2\rho^2-1$ in Sec. 10.2.37. From Ref. 14, Secs. 22.14.7 and 10.25,

$$|R_{2n}^0(\rho)|\leq 1,\quad \sqrt{\frac{\pi}{\alpha}}I_{n+1/2}(\alpha/2)\approx\frac{(\alpha/2)^n}{1\times 3\cdots(2n+1)},\quad n\to\infty. \tag{A3}$$

For instance, when $\alpha=1$, including the terms in the series in Eq. (A2) with $n=0,\ldots,5$ yields absolute accuracy $10^{-6}$ on the whole range $0\leqslant\rho\leqslant 1$. Alternatively, there is an expansion in terms of the velocity profiles $(1-(\sigma/a)^2)^n$ of Eq. (6), viz.,

$$e^{-\alpha\rho^2}=e^{-\alpha}\sum_{n=0}^{\infty}\frac{\alpha^n}{n!}(1-\rho^2)^n. \tag{A4}$$

Denoting the expansion coefficients in Eq. (A2) by $u_n$ and those in Eq. (A4) by $w_n$, it follows from the asymptotics of the $\Gamma$-function that

$$\frac{u_n}{w_n}\approx e^{(1/2)\alpha}\frac{\sqrt{\pi n}}{4^n},\quad n\to\infty. \tag{A5}$$

Thus the $n$th coefficient required in the clamped radiator expansion in Eq. (A4) is roughly $4^n$ as large as the one needed in the Zernike expansion in Eq. (A2). This phenomenon has been noted and verified for a large set of other analytic velocity profiles such as (spherical) Bessel functions.

### 3. Expansion of $\exp(-i\lambda(T^2+x\rho^2)^{1/2})/-i\lambda(T^2+x\rho^2)^{1/2}$

To show Eq. (12), consider Ref. 14, Secs. 10.1.45 and 10.1.46,

$$\frac{e^{i\lambda V}}{i\lambda V} = \sum_{n=0}^{\infty} (2n+1) j_n(\lambda r_1) h_n^{(1)}(\lambda r_2) P_n(\cos\gamma), \tag{A6}$$

where $V=(r_1^2+r_2^2-2r_1r_2\cos\gamma)^{1/2}$ with $\gamma\in\mathbb{R}$, and $0\leqslant|r_1|\leqslant r_2$. With the choice

$$r_1 = T_-, \quad r_2 = T_+, \quad \cos\gamma = 1-2\rho^2, \tag{A7}$$

one has $V=(T^2+x\rho^2)^{1/2}$ and Eq. (12) follows using $P_n(-x)=(-1)^nP_n(x)$, $R_{2n}^0(\rho)=P_n(2\rho^2-1)$ and Ref. 14, Secs. 10.1.1, 10.1.3,

$$j_n(-z) = (-1)^n j_n(z), \quad h_n^{(1)}(-z) = (-1)^n h_n^{(2)}(z). \tag{A8}$$

## APPENDIX B: FAR-FIELD APPROXIMATION

Letting $\underline{r}=(r\sin\theta,0,r\cos\theta)$, it holds

$$p(\underline{r}) = \frac{i\rho_0 ck}{2\pi}\int_S v(\underline{r}_s)\frac{e^{-ikr'}}{r'}dS = i\rho_0 ck\int_0^a v(\sigma) \times\left(\frac{1}{2\pi}\int_0^{2\pi}\frac{e^{-ik\sqrt{r^2+\sigma^2-2r\sigma\sin\theta\cos\varphi}}}{\sqrt{r^2+\sigma^2-2r\sigma\sin\theta\cos\varphi}}d\varphi\right)d\sigma. \tag{B1}$$

Now, when $r\to\infty$,

$$\sqrt{r^2+\sigma^2-2r\sigma\sin\theta\cos\varphi} \approx r-\sigma\sin\theta\cos\varphi \approx r. \tag{B2}$$

Replacing $r'$ in $\exp(-ikr')$ with $r-\sigma\sin\theta\cos\varphi$ and $r'$ in the denominator in the integrand in Eq. (B1) with $r$ while using

$$\int_0^{2\pi} e^{iz\cos\varphi}d\varphi = 2\pi J_0(z), \tag{B3}$$

the conventional approximation

$$p(\underline{r}) \approx i\rho_0 ck\frac{e^{-ikr}}{r}\int_0^a v(\sigma)J_0(k\sigma\sin\theta)\sigma d\sigma \tag{B4}$$

follows. Then Eq. (27) follows upon inserting in Eq. (B4) the Zernike expansion (3) of $v$ and using the result of Eq. (14).

## APPENDIX C: ON-AXIS FIELD FOR A DOME-SHAPED RADIATOR

In this appendix the result of Eqs. (46)–(49) is proved. The on-axis pressure at $\underline{r}=(0,0,r)$ is given by, see Eq. (45),

$$p(\underline{r}) = i\rho_0 ck\int_0^a \frac{bv(\sigma)}{\sqrt{b^2-\sigma^2}}\frac{e^{-ikr'}}{r'}\sigma d\sigma, \tag{C1}$$

in which

$$r' = (r^2+\sigma^2-2rd(\sigma)+d^2(\sigma))^{1/2} \tag{C2}$$

and $d(\sigma)$ is given by Eq. (40). Working this out, while noting cancellation of terms $\sigma^2$ due to the special form of $d$, it follows that

$$(r')^2 = c(r)+d(r)\psi(\sigma), \quad \psi(\sigma) = -(b^2-\sigma^2)^{1/2}, \tag{C3}$$

where $c(r)$ and $d(r)$ only depend on $r$. In normalized coordinates

$$\rho=\sigma/a, \quad s_0=a/b, \tag{C4}$$

Eq. (C3) assumes the form

$$(r'/a)^2 = C(r)+D(r)\Psi(\rho) =: F(\rho;r), \tag{C5}$$

where $C(r)=a^{-2}c(r)$, $D(r)=a^{-2}d(r)$, and

$$\Psi(\rho) = \frac{1}{b}\psi(\sigma) = -(1-s_0^2\rho^2)^{1/2}, \quad 0\leq\rho\leq 1. \tag{C6}$$

This $F(\rho;r)$ can be written as

$$F(\rho;r) = F(0;r)+(F(1;r)-F(0;r))f^2(\rho), \tag{C7}$$

where

$$f(\rho) = \sqrt{\frac{\Psi(\rho)-\Psi(0)}{\Psi(1)-\Psi(0)}} = \sqrt{\frac{1-(1-s_0^2\rho^2)^{1/2}}{1-c_0}} \tag{C8}$$

and $c_0=(1-s_0^2)^{1/2}$. Letting

$$T^2 = F(0;r), \quad x = F(1;r)-F(0;r), \tag{C9}$$

it follows that $r'=a(T^2+xf^2(\rho))^{1/2}$. Hence, from Eqs. (C1) and (12) with $\lambda=ka$ and $f(\rho)$ instead of $\rho$,

$$p(\underline{r}) = i\rho_0 cka\int_0^1 \frac{v(a\rho)}{\sqrt{1-s_0^2\rho^2}}\frac{e^{-ikr'}}{r'}\rho d\rho = \rho_0 c(ka)^2\sum_{n=0}^{\infty}\delta_n(k,r)t_n, \tag{C10}$$

in which, see below Eq. (12),

$$\delta_n(k,r) = (-1)^n j_n(kaT_-)h_n^{(2)}(kaT_+) \tag{C11}$$

and

$$t_n = (2n+1)\int_0^1 \frac{v(a\rho)}{\sqrt{1-s_0^2\rho^2}}R_{2n}^0(f(\rho))\rho d\rho. \tag{C12}$$

From Eqs. (C5) and (C9) it follows that

$$aT = r-d(0), \quad a\sqrt{T^2+x} = \sqrt{r^2+a^2}; \tag{C13}$$

hence, $\delta_n(k,r)$ is given by the RHS of Eq. (49). Next, substitute $\tau=f(\rho)$, $\rho=g(\tau)$ in the integral defining $t_n$, where the inverse function $g$ of $f$ is given by

$$g(\tau) = \tau\left(\frac{2-(1-c_0)\tau^2}{1+c_0}\right)^{1/2}, \quad 0\leq\tau\leq 1. \tag{C14}$$

Then, using

$$\frac{g'(\tau)g(\tau)}{\sqrt{1-s_0^2g^2(\tau)}} = \frac{2}{1+c_0}, \tag{C15}$$

it follows that

$$t_n = \frac{2(2n+1)}{1+c_0}\int_0^1 v(ag(\tau))R_{2n}^0(\rho)\rho d\rho. \tag{C16}$$

Noting that $W(\tau)=v(ag(\tau))$, see Eq. (47), the proof is complete.

[1]G. R. Harris, "Review of transient field theory for a baffled planar piston," J. Acoust. Soc. Am. **70**, 10–20 (1981).
[2]M. Greenspan, "Piston radiator: Some extensions of the theory," J. Acoust. Soc. Am. **65**, 608–621 (1979).
[3]T. D. Mast and F. Yu, "Simplified expansions for radiation from a baffled circular piston," J. Acoust. Soc. Am. **118**, 3457–3464 (2005).
[4]T. B. Hansen, "Probe-corrected near-field measurements on a truncated cylinder," J. Acoust. Soc. Am. **119**, 792–807 (2006).
[5]T. J. Mellow, "On the sound field of a resilient disk in an infinite baffle," J. Acoust. Soc. Am. **120**, 90–101 (2006).
[6]J. F. Kelly and R. J. McGough, "An annular superposition integral for axisymmetric radiators," J. Acoust. Soc. Am. **121**, 759–765 (2007).
[7]B. R. A. Nijboer, "The diffraction theory of aberrations," Ph.D. dissertation, University of Groningen, The Netherlands, 1942.
[8]F. Zernike and B. R. A. Nijboer, "The Theory of Optical Images (La théorie des images optiques), Revue d'Optique, Paris, 227–235 (1949).
[9]M. Born and E. Wolf, *Principles of Optics*, 7th ed. (Cambridge University Press, Cambridge, 2002), Chap. 9.
[10]J. J. M. Braat, S. van Haver, A. J. E. M. Janssen, and P. Dirksen, "Assessment of optical systems by means of point-spread functions," in *Progress in Optics*, edited by E. Wolf (Elsevier, Amsterdam, 2008), Vol. **51**, Chap. 6.
[11]L. E. Kinsler, A. R. Frey, A. B. Coppens, and J. V. Sanders, *Fundamentals of Acoustics* (Wiley, New York, 1982).
[12]J. W. S. Rayleigh, *The Theory of Sound* (The Macmillan Co., London, 1896), Vol. **2**; *ibid.* (Dover, New York, 1945).
[13]F. J. M. Frankort, "Vibration and sound radiation of loudspeaker cones," Ph.D. dissertation, Delft University of Technology, Delft, The Netherlands, 1975.
[14]M. Abramowitz and I. A. Stegun, *Handbook of Mathematical Functions* (Dover, New York, 1972).
[15]H. Stenzel, "On the acoustical radiation of membranes (Über die akustische strahlung von membranen)," Ann. Phys. **7**, 947–982 (1930).
[16]D. L. Dekker, R. L. Piziali, and E. Dong, "Effect of boundary conditions on the ultrasonic-beam characteristics of circular disks," J. Acoust. Soc. Am. **56**, 87–93 (1974).
[17]D. B. (Don) Keele, Jr., "Low-frequency loudspeaker assessment by nearfield sound-pressure measurement," J. Audio Eng. Soc. **22**, 154–162 (1974).
[18]International Electrotechnical Commission (IEC), Geneva, Switzerland, IEC 60268-5 Sound System Equipment—Part 5: Loudspeakers, 2007.
[19]G. H. Golub and C. F. Van Loan, *Matrix Computations*, 2nd ed. (The Johns Hopkins University Press, Baltimore, MD, 1989).
[20]P. G. Bordoni, "The conical sound source," J. Acoust. Soc. Am. **17**, 123–126 (1945).
[21]J. M. Kates, "Radiation from a dome," J. Audio Eng. Soc. **24**, 735–737 (1976).
[22]H. Suzuki and J. Tichy, "Sound radiation from convex and concave domes in an infinite baffle," J. Acoust. Soc. Am. **69**, 41–49 (1981).
[23]J. J. M. Braat, P. Dirksen, A. J. E. M. Janssen, and A. S. van de Nes, "Extended Nijboer-Zernike representation of the vector field in the focal region of an aberrated high-aperture optical system," J. Opt. Soc. Am. A **20**, 2281–2292 (2003).